Optics and Laser Technology 101 (2018) 379–387

Contents lists available at ScienceDirect

Optics and Laser Technology

journal homepage: www.elsevier.com/locate/optlastec

Full length article

Highly sensitive LSPR based photonic crystal fiber sensor with embodiment of nanospheres in different material domain

D. Paul, R. Biswas *

Applied Optics and Photonics Laboratory, Department of Physics, Tezpur University, Napaam, Sonitpur 784028, India

ARTICLE INFO

Article history:
Received 11 September 2017
Received in revised form 22 November 2017
Accepted 24 November 2017

Keywords:
Localized surface plasmon resonance (LSPR)
Photonic crystal fiber (PCF)
Nanospheres

ABSTRACT

We report a highly sensitive Localized surface plasmon resonance (LSPR) based photonic crystal fiber (PCF) sensor by embedding an array of gold nanospheres into the first layer of air-holes of PCF. We present a comprehensive analysis on the basis of progressive variation of refractive indices of analytes as well as sizes of the nanospheres. In the proposed sensing scheme, refractive indices of the analytes have been changed from 1 to 1.41(RIU), accompanied by alteration of the sizes of nanospheres ranging 40–70 nm. The entire study has been executed in the context of different material based PCFs (*viz.* phosphate and crown) and the corresponding results have been analyzed and compared. We observe a declining trend in modal loss in each set of PCFs with increment of RI of the analyte. Lower loss has been observed in case of crown based PCF. The sensor shows highest sensitivity ~27,000 nm/RIU for crown based PCF for nanosphere of 70 nm with average wavelength interrogation sensitivity ~5333.53 nm/RIU. In case of phosphate based PCF, highest sensitivity is found to be ~18,000 nm/RIU with an average interrogation sensitivity ~4555.56 nm/RIU for 40 nm of Au nanosphere. Moreover, the additional sensing parameters have been observed to highlight the better design of the modelled LSPR based photonic crystal fiber sensor. As such, the resolution (R), limit of detection (LOD) and sensitivity (S) of the proposed sensor in each case (viz. phosphate and crown PCF) have been discussed by using wavelength interrogation technique. The proposed study provides a basis for detailed investigation of LSPR phenomenon for PCF utilizing noble metal nanospheres (AuNPs).

1. Introduction

The optical properties of noble metal nanoparticles can be studied based on localized surface plasmon resonance (LSPR) phenomenon which is adopted in multitude of applications [1–4]. LSPR based sensors have caught much attention of researchers during the past few years owing to their controlled/optimized techniques [3]. LSPR phenomenon arises because of collective oscillations of conduction band electrons. These oscillations occur at nanoparticles interface, when excited by incident light of suitable wavelength. At resonance, coupling of the incident electromagnetic radiation with the nanoparticles takes place, which is indicated by a strong absorption of a specific frequency (resonance frequency) of the incident light [4]. Besides, the resonance frequency has been found to have strong dependence with its size, shapes and even the refractive indices of the surrounding media have also a great impact on resonance frequency of noble metal nano particles [3–5]. Further, LSPR based sensing scheme can be more functional with the use of suitable optical platform. Towards this, photonic crystal fiber (PCF) offers several advantages over the conventional fiber. The design flexibility of photonic crystal fiber (PCF) enables it to support a number of applications over conventional fiber [6–8]. Due to such tunable configurational properties of PCF, they are now being widely implemented in sensing applications based on surface plasmons [4,5]. Although surface plasmon based PCFs have been studied, but, very few theoretical and experimental works have been reported on LSPR based PCF sensors [4,5]. Till date Zhou [4] and Yang et al. [5] have introduced LSPR based sensor utilizing PCF. As a matter of fact, LSPR based PCF sensor requires a detailed theoretical framework which will eventually lead to different practical implementations. Additionally, alteration of structural and modal parameters of PCFs, entailing noble metal nanoparticles leads to considerable shifts in plasmonic bands, thereby affecting the sensitivity. The sensitivity enhancement with tuning of nanoparticles and structural parameters of PCF in particular need a comprehensive analysis.

With these objectives, we attempt to study here the sensing performances of our proposed LSPR based PCF sensors. We analyze

* Corresponding author.
E-mail addresses: dmppaul22@gmail.com (D. Paul), rajib@tezu.ernet.in (R. Biswas).

https://doi.org/10.1016/j.optlastec.2017.11.040
0030-3992/

the responses in terms of varying sizes of Au nanospheres which are embedded into the first layer of air holes of PCF. We introduce analytes of different RI in the surrounding medium of this embedded layer of Au nanospheres. Correspondingly, we perform the sensitivity analysis of this prototype by incorporating phosphate and crown as the constituent of the PCFs. It is worthwhile to note that we have already reported modal parameter study on PCF in the context of two different materials *viz.* phosphate and crown [9–11]. Additionally, dependence of modal loss (α_{loss}) [12,13] with significant change in the RI (n) of the analyte with resonant wavelength (λ) has been demonstrated in this work. Detection of unknown analyte corresponding to various refractive indices can also be implemented over embedded nanospheres. Besides, the loss has also been analyzed in the context of different material based PCFs (*viz.* phosphate and crown).

2. Theoretical demonstration

During the study, the numerical simulation has been performed by considering nanospheres of different sizes, ranging from 40 to 70 nm with an increment of 10 nm. Furthermore, the excitation has been performed by changing RI of the analytes ranging 1.32–1.41 (RIU). Fig. 1 shows cross sectional view of the proposed LSPR sensor. The diameter of the core is considered to be 4 μm along with the air hole spacing of ~3.5 μm and air hole diameter of ~2.3 μm. Besides, the proposed structure has been chosen owing to its optimum space filling factor, which is less than 0.6. The space filling factor is considered as the largest mode index which effectively contributes to the effective refractive index of the cladding [14,15]. Thus, the optimal space filling mode is essential to control the losses during sensing application. During the analysis the filling factor is considered to be 0.6 to obtain optimum modal loss with implementation of nanospheres as per reports Midrio et al. [14] and Li et al. [15]. In hexagonal lattice pattern, the proposed sensing scheme comprises of seven layers of air holes. The first layer of air holes has been replaced by a regular array of Au nanospheres. This first layer of embedded Au nanospheres acts as the sensing region. The LSPR responses are observed with change in the RI of the analytes in the surrounding from 1.32 to 1.41. We incorporate two PCFs (*viz.* phosphate and crown) and accordingly, the sensitivity has been estimated with respect to these PCFs. The peak absorption wavelength has been evaluated from the loss spectra with respective change in sizes of the nanospheres and for each size, a comprehensive analysis has been made. The sensitivity of the sensor has been illustrated in terms of the loss peak resonance wavelength per unit change in RI. The core RI ~ 1.59 has been considered for crown based PCF and ~1.56 for phosphate based PCF. The cladding refractive indices are dependent on the refractive index of the core and the refractive index of the glass material used. Moreover, the sensitivity has been observed based on Eq. (2) which is dependent on peak absorption wavelength λ_{peak} and the change in refractive index on the vicinity of the embedded nanospheres.

During the study, modal loss of the proposed structure has also been calculated by using the following Eq. in the context of two different material regime (*viz.* phosphate and crown) [12,13,16–19]:

$$\alpha_{loss} = \frac{40\pi}{\lambda \ln(10)} Im(n_{eff}) \approx 8.686 \times k_0 \times Im(n_{eff}) \times 10^6 \ (\mathrm{dB/m}) \quad (1)$$

In which, k_0 ($2\pi/\lambda$) is the wavenumber with 'Im (n_{eff})' is the imaginary part of the effective refractive index of the photonic crystal fiber. The wave-number is given by $\frac{1}{1.55}$ in terms of $(\mu m)^{-1}$. The modal loss has been evaluated in the context of different sized nanosphere in presence of different analytes with variable RI. Furthermore, to check the sensing performance of the proposed sensor, the spectral sensitivity, resolution and LOD have also been evaluated using the following equations [12,14–17]:

$$\text{Spectral sensitivity}: \ S(\lambda) = \frac{\Delta\lambda_{peak}}{\Delta n_a} \ (\mathrm{nm/RIU}) \quad (2)$$

$$\text{Resolution}: \ R = \left(\frac{\Delta n_a \times \lambda_{\min}}{\Delta\lambda_{peak}}\right) \quad (3)$$

$$\text{Limit of detection (LOD)}: \ \mathrm{LOD} = \left(\frac{R}{S}\right) \quad (4)$$

where $\Delta\lambda_{peak}$ and Δn_a are the peak shift in resonance wavelength and variation in the RI of the proposed analytes, respectively and S refers to the spectral sensitivity.

The block diagram of the formulation used in LSPR-PCF sensor has been provided below:

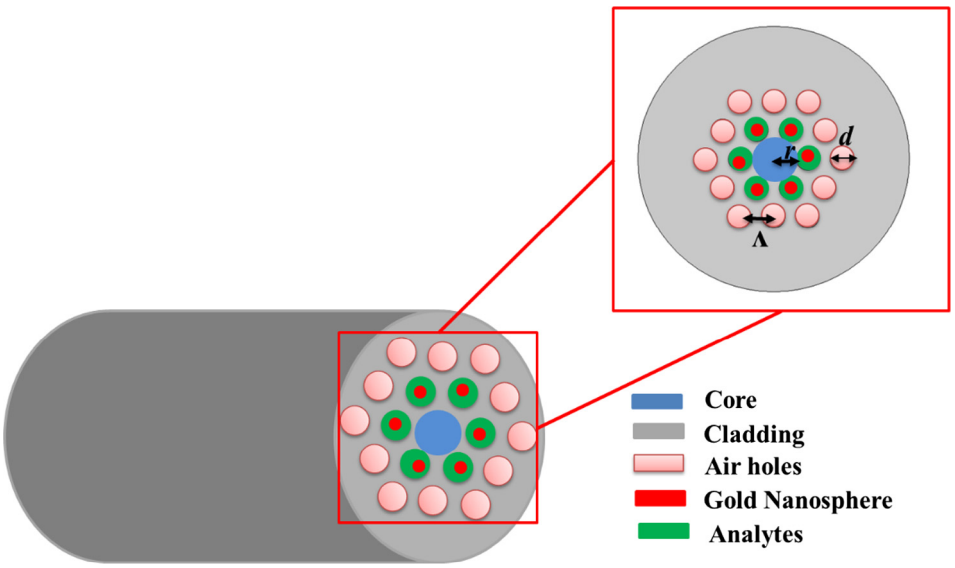

Fig. 1. Schematic of photonic crystal fiber in which the first layer of air holes shows the embedded gold nanosphere and respective analytes with variable RI.

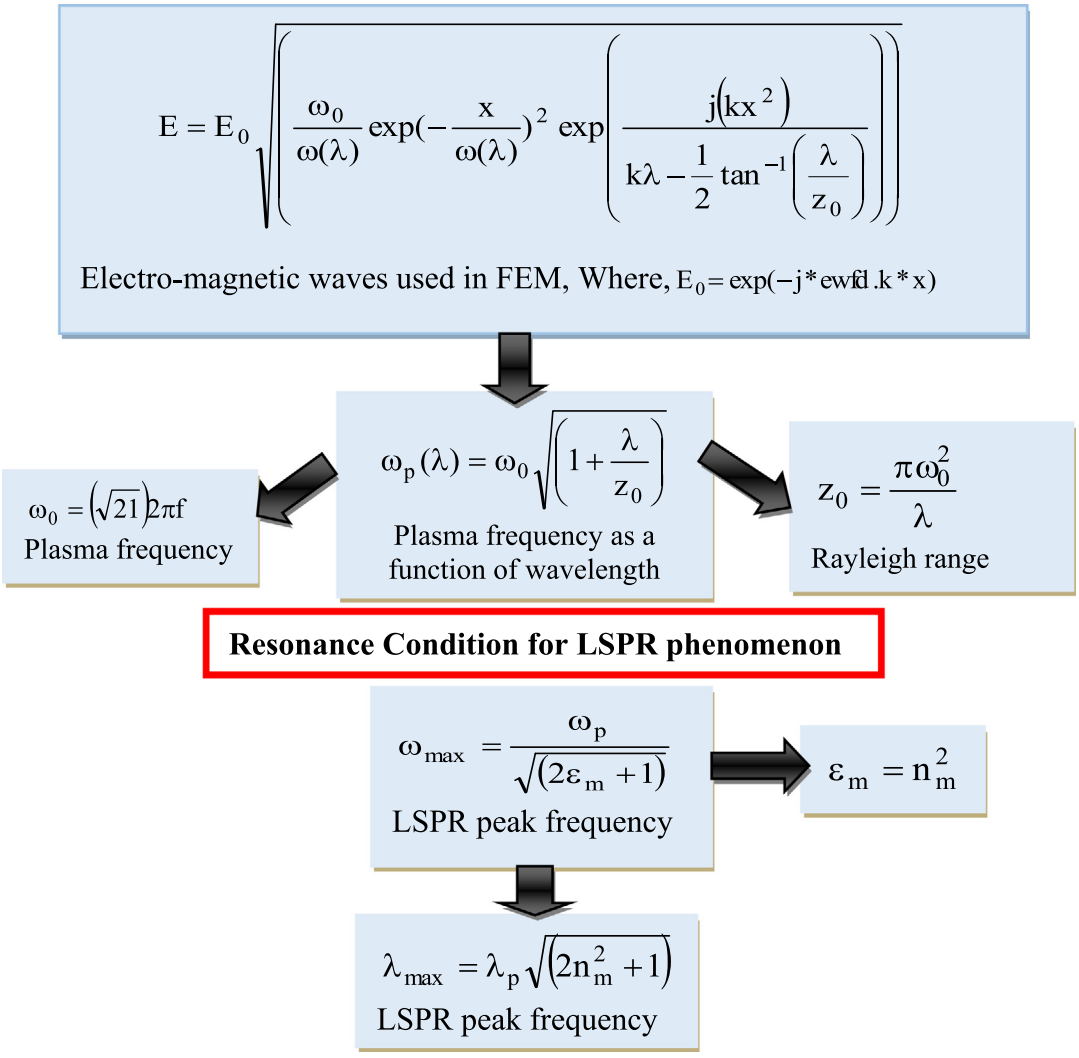

The proposed structure is 2-dimensional LSPR-PCF sensor. To ensure the model of LSPR sensor, a flowchart has been provided in the text as '*Structural design and formulation*' as a block diagram. 'The block diagram of the formulation used in LSPR-PCF sensor' describes the overall formulation that has been used during the analysis. Here, the finite element method has been utilized to study the sensing performance of LSPR-PCF analysis.

3. Results and discussion

In this work, we present a detailed study of LSPR in the context of phosphate and crown based PCF. To attain this objective, we fabricate an array of Au nanospheres of different sizes ~40–70 nm onto the first layer of air holes of PCF. The interaction between leaky core modes with surface plasmons leads to resonance which ultimately yields different responses due to alteration of surrounding medium. Accordingly, the responses with respect to varying sizes of nanosphere and incremental change in RI of the analytes are observed and analyzed. The resonance has been achieved in the proposed LSPR-PCF sensor by considering the interaction between the leaky core modes with the plasmons [14]. The resonance occurs only when the leaky core mode excites the surface plasmons of the embedded Au nanospheres and thereby leads to corresponding LSPR responses. Eventually, the phase matching condition for PCF occurs between the effective refractive index of core mode and the plasmonic modes [13]. The sensor is found to be sensitive with incremental change in RI as well as the sizes of nanosphere. Fig. 2(a)–(d) illustrate modal loss versus λ for phosphate PCF and it has been observed that with progressive rise in RI of analytes, the loss undergoes a red shift. Moreover, the loss spectrum of each nanosphere of sizes 40–70 nm is found to decrease gradually from 99.46 to 52.67 dB/m for phosphate based PCF. Similar pattern has been observed in case of crown based PCF which is illustrated in Fig. 3(a)–(d). In similitude to phosphate PCF, the losses with respective change in sizes and RI exhibit to red shift. With change in sizes of nanosphere from 40 to 70 nm, the losses in case of crown based PCF are found to decrease from 92.1 to 68.56 dB/m (Fig. 3). Here, wavelength interrogation technique [13] has been followed to describe the response of the proposed sensor. In case of phosphate PCF (Fig. 2), a maximum refractive index sensitivity of ~18,000 nm/RIU (Eq. (2)) has been obtained for 40 nm nanosphere with maximum loss of ~99.46 dB/m at 690 nm. Modal loss ~33.84 dB/nm is found to be at 1130 nm for RI-1.41 that exhibits declining trend with increase in RI. Moreover, the resonant losses for phosphate PCF are found to be ~88.41, 77.50, 65.35, 59.35, 48.14, 40.93, 37.52, 35.24 and 34.35 dB/m for RI-1.32–1.40 with resonance peak λ at 710, 770, 780, 800, 980, 1010, 1040, 1080 and 1110 nm respectively (40 nm nanosphere). Likewise, in case of crown based PCF an, increment in RI of the surrounding media leads to the variation in the resonance condition in similitude to phosphate PCF. Further, in crown PCF, the modal losses are found to decline from 70.95,

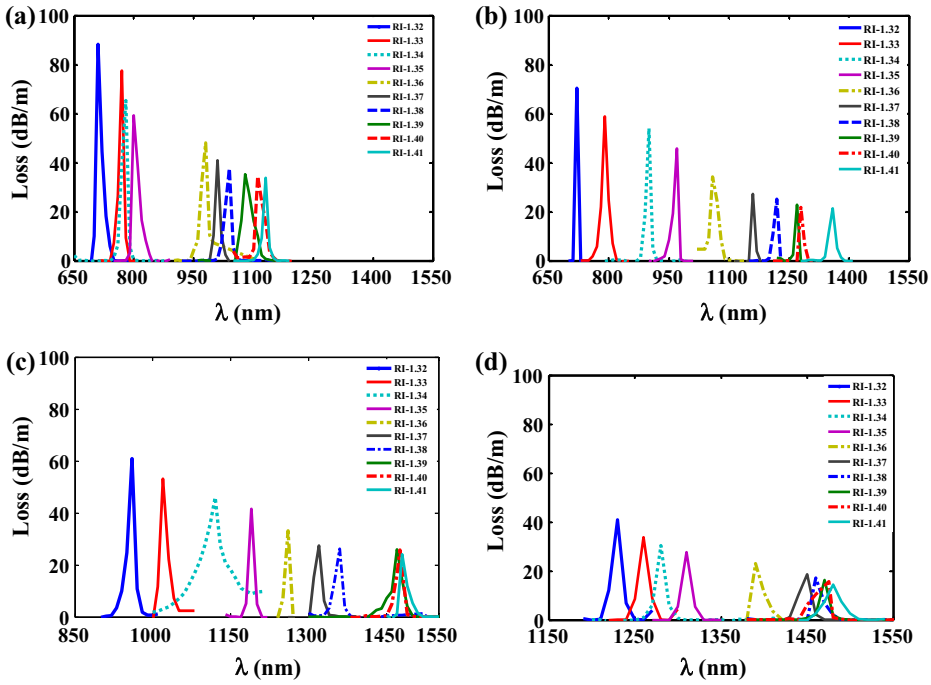

Fig. 2. Loss spectrum vs. λ of the proposed sensor by varying RI and size of nanospheres as (a) 40 nm, (b) 50 nm, (c) 60 nm and (d) 70 nm for phosphate based PCF.

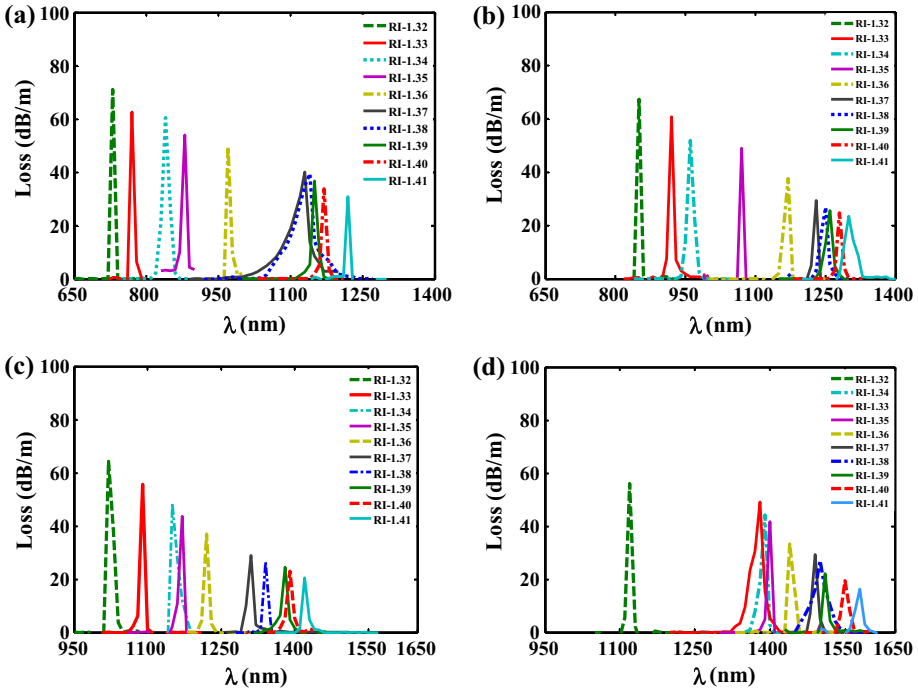

Fig. 3. Loss spectrum vs. λ of the proposed sensor by varying RI and size of nanospheres as (a) 40 nm, (b) 50 nm, (c) 60 nm and (d) 70 nm for crown based PCF.

62.63, 60.58, 54.03, 49.50, 40.11, 39.57, 36.84, 33.73 and 30.75 dB/m for RI-1.32–1.41 with resonance peak λ_{peak} at 730, 770, 840, 880, 970, 1130, 1140, 1150, 1170 and 1220 nm, respectively for 40 nm nanosphere. As observed in Figs. 2 and 3, modal loss of the proposed structure decrease with increase in RI of analytes surrounding to the nanospheres. The lowering of modal loss is due to higher penetration of electromagnetic filed towards the core and lower penetration towards the surface of nanosphere. Thus, the variation in loss correspondingly changes the sensitivity of the proposed structure. In Table 1, the peak resonance wavelengths and additional sensing parameters have been enlisted for both phosphate and crown based PCF.

Figs. 4 and 5 illustrate the consistency of the proposed sensor performance in the context of phosphate and crown PCF for RI of

Table 1
Sensing performance of the proposed sensor.

Size of NPs	Analytes RI	Resonance λ_{peak} (nm)		Loss (dB/nm)		Sensitivity (S) (nm/RIU)		Resolution (R) (RIU)		LOD = R/S	
		Phosphate based PCF	Crown based PCF	Phosphate based PCF	Crown based PCF	Phosphate based PCF	Crown based PCF	Phosphate based PCF	Crown based PCF	Phosphate based PCF	Crown based PCF
40 nm	–	690	690	99.46	92.1	–	–				
	1.32	710	730	88.41	70.95	6000	4000				
	1.33	770	770	77.5	62.63	1000	7000				
	1.34	780	840	65.35	60.58	2000	4000				
	1.35	800	880	59.35	54.03	2000	9000	5.56×10^{-6}	6.25×10^{-6}	3.09×10^{-10}	3.91×10^{-10}
	1.36	980	970	48.14	49.5	18,000	16,000				
	1.37	1010	1130	40.93	40.11	3000	1000				
	1.38	1040	1140	37.52	39.57	4000	1000				
	1.39	1080	1150	35.24	36.84	3000	2000				
	1.40	1110	1170	34.35	33.73	2000	5000				
	1.41	1130	1220	33.84	30.75						
50 nm	–	700	730	86.5	88.62	–	–				
	1.32	720	850	70.34	67.19	7000	7000				
	1.33	790	920	58.94	60.72	11,000	4000	9.09×10^{-6}	6.67×10^{-6}	8.26×10^{-10}	4.45×10^{-10}
	1.34	900	960	53.98	51.86	7000	6000				
	1.35	970	1020	45.84	48.87	9000	15,000				
	1.36	1060	1170	34.11	37.49	10,000	6000				
	1.37	1160	1230	27.23	29.47	6000	2000				
	1.38	1220	1250	25.21	26.87	5000	1000				
	1.39	1270	1260	22.75	25.59	1000	2000				
	1.40	1280	1280	21.83	24.77	8000	2000				
	1.41	1360	1300	21.46	23.58						
60 nm	–	880	960	71.49	75.72	–	–				
	1.32	960	1020	60.91	64.26	6000	7000				
	1.33	1020	1090	53.07	55.67	10,000	6000				
	1.34	1120	1150	46.05	48.23	7000	2000	9.09×10^{-6}	1.12×10^{-5}	8.26×10^{-10}	1.24×10^{-9}
	1.35	1190	1170	41.53	43.66	7000	5000				
	1.36	1260	1220	33.15	37	6000	9000				
	1.37	1320	1310	27.54	28.9	4000	3000				
	1.38	1360	1340	26.11	26.4	11,000	4000				
	1.39	1470	1380	25.95	24.62	500	1000				
	1.40	1475	1390	25.72	23.02	500	3000				
	1.41	1480	1420	24.06	20.52						
70 nm	–	1030	1100	52.67	68.56	–	–				
	1.32	1230	1120	40.88	56.05	3000	27,000				
	1.33	1260	1380	33.79	49.12	2000	1000				
	1.34	1280	1390	30.47	44.34	3000	2000				
	1.35	1310	1400	27.72	41.86	8000	4000	1.60×10^{-4}	3.70×10^{-6}	2.0×10^{-8}	1.37×10^{-10}
	1.36	1390	1440	23.09	33.43	6000	5000				
	1.37	1450	1490	18.54	29.47	1000	1000				
	1.38	1460	1500	17.05	27.14	1000	1000				
	1.39	1470	1510	16.36	22.31	500	4000				
	1.40	1475	1550	15.76	19.52	500	3000				
	1.41	1480	1580	14.49	16.21						

1.32–1.41. It is evident that Figs. 4 and 5 show a declining trend for loss profile vs. RI and a rising trend for resonance peak wavelength vs. RI. However, both phosphate and crown PCFs are characterized by resonance shifts with goodness of fit $R^2 \approx 1$. This validates the linearity of the responses received. Additionally, the sensitivity can be further defined by incorporation of parameters such as resolution and limit of detection (LOD) [17,18] (Eqs. (3) and (4)) which control the extent to which the sensor can precisely detect small changes in sizes and nearby RI. By following White et al. and Rifat et al. [17,18] the resolution of the proposed sensor has been analyzed and values are enlisted in Table 1. Figs. 4 and 5 show that the modal loss (supplementary material Table S-1) of plasmonic sensors increases with increase in penetration of electromagnetic fields towards the metal layer [20]. In this case, modal losses decrease with decease in penetration of electro-magnetic field towards the nanosphere surface and correspondingly, they decline with respective change in RI of the analytes.

The variation in the peak resonance wavelength with respective change in RI of the analytes for 40–70 nm nanospheres in phosphate based PCF can be represented by the following empirical equations:

$$\left.\begin{aligned}
&40\text{ nm}: \ \lambda_{peak}(n) = 3.4 \times 10^3 n - 3.7 \times 10^3 \text{ and } Loss_{peak}(n) \\
&\quad = 3.4 \times 10^2 - 2.2 \times 10^2 n \\
&50\text{ nm}: \ \lambda_{peak}(n) = 4.1 \times 10^3 n - 4.5 \times 10^3 \text{ and } Loss_{peak}(n) \\
&\quad = 2.8 \times 10^2 - 1.9 \times 10^2 n \\
&60\text{ nm}: \ \lambda_{peak}(n) = 5.7 \times 10^3 n - 6.5 \times 10^3 \text{ and } Loss_{peak}(n) \\
&\quad = 7.4 \times 10^2 - 5.2 \times 10^2 n \\
&70\text{ nm}: \ \lambda_{peak} = 8.5 \times 10^2 n + 2.9 \times 10^2 \text{ and } Loss_{peak}(n) \\
&\quad = 1.4 \times 10^2 - 90.3n
\end{aligned}\right\} \quad (5)$$

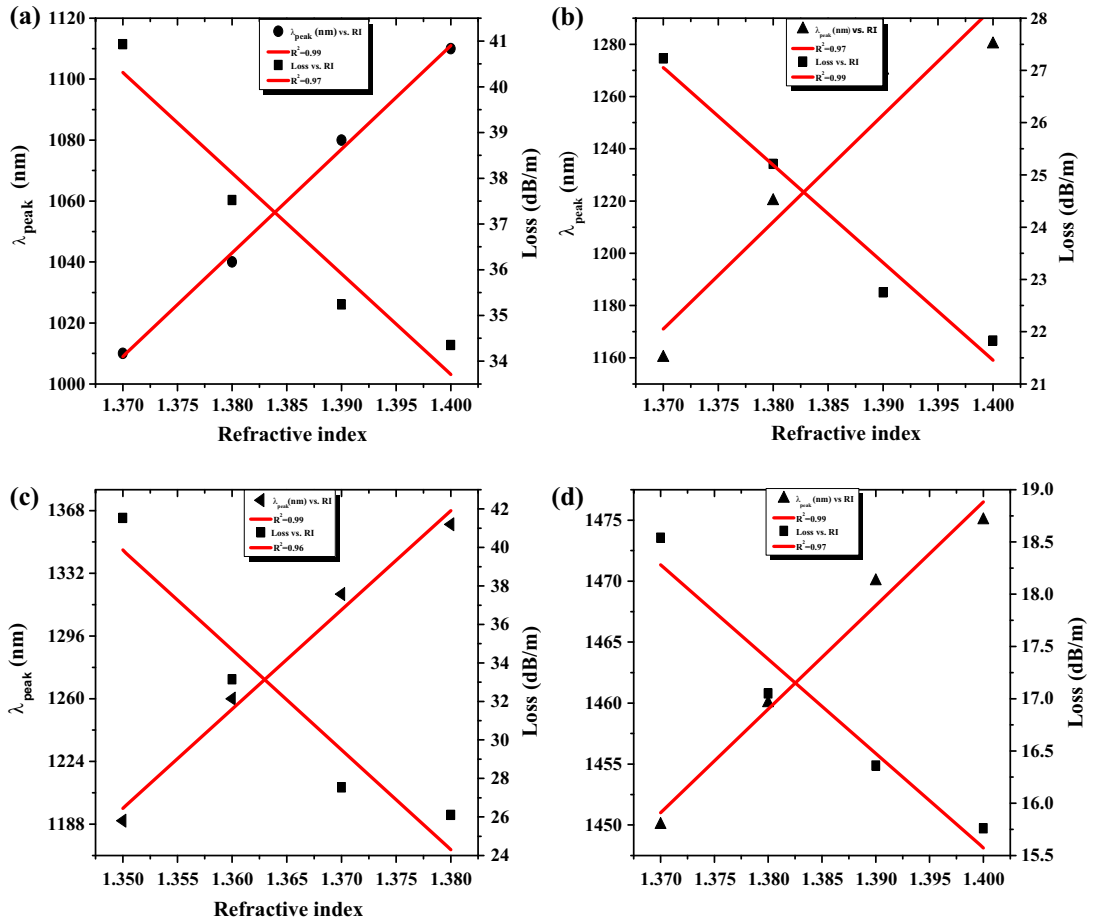

Fig. 4. Linear fitting curves for λ_{peak} and their corresponding loss vs. RI (1.37–1.40) of (a) 40 nm, (b) 50 nm, (c) 60 nm and (d) 70 nm nanospheres for phosphate based PCF.

Similarly, variation observed in crown PCF with respective change in RI of the analyte with size of the nanospheres can be described by the empirical equations which are as follows:

$$\left.\begin{aligned} &40\text{ nm}: \lambda_{peak}(n) = 1.3\times10^3 n - 6.5\times10^2 \text{ and } Loss_{peak}(n) \\ &\quad = 3.4\times10^2 - 2.2\times10^2 n \\ &50\text{ nm}: \lambda_{peak}(n) = 1.6\times10^3 n - 9.6\times10^2 \text{ and } Loss_{peak}(n) \\ &\quad = 2.4\times10^2 - 1.5\times10^2 n \\ &60\text{ nm}: \lambda_{peak}(n) = 2.8\times10^3 n - 2.5\times10^3 \text{ and } Loss_{peak}(n) \\ &\quad = 2.9\times10^2 - 1.9\times10^2 n \\ &70\text{ nm}: \lambda_{peak}(n) = 2.8\times10^3 n - 2.3\times10^3 \text{ and } Loss_{peak}(n) \\ &\quad = 1.4\times10^2 - 90.3n \end{aligned}\right\} \quad (6)$$

Fig. 6(a) and (b) illustrates modal loss of the proposed sensor with respective change in sizes of nanospheres from 40 to 70 nm with an increment of 10 nm. It has been observed that with gradual increment in size of nanosphere, the corresponding losses decrease for both the phosphate and crown PCF in Fig. 6(c) and (d). Besides, in both the PCFs (*viz.* phosphate and crown), the resonance shifts yield a squared of regression, $R^2 \approx 1$; thus establishing linearity of the proposed sensor with respect to the variation in sizes of nanospheres.

Additionally, the variation of each PCF's with respective change in size of the nanosphere can be empirically written as:

$$\left.\begin{aligned} &\text{Phosphate}: \lambda_{peak}(n') = 12n' + 165 \text{ and } Loss_{peak}(n') \\ &\quad = 162.99 - 1.6n' \\ &\text{Crown}: \lambda_{peak}(n') = 11.9n' + 193 \text{ and } Loss_{peak}(n') \\ &\quad = 127.19 - 0.84n' \end{aligned}\right\} \quad (7)$$

In Fig. 7(a), a very sharp peak has been observed at $\lambda \sim 710$ nm for phosphate PCF for nanosphere size of 40 nm. This wavelength corresponds to the matching of the effective refractive index of the fundamental core mode with surface plasmon mode. This ensured the maximum power transfer from core mode to the plasmon mode. Thus, at resonance, the proposed sensor provides the reasonable sensing performance. Similarly, Fig. 7 (b) also describes the phase matching condition of the fundamental core mode, surface plasmon mode and that with the Im (n_{eff}) at $\lambda \sim 730$ nm, corresponding to crown PCF. In similitude to phosphate PCF we analyze dispersion relation for crown PCF, for nanosphere array of diameter; 40 nm. The insets *viz.* (a)–(c) of Fig. 7(a) and (b) shows the electric field distribution of (a) core mode (b) at resonance with (c) plasmon mode, respectively. The sensing performance of each set of PCFs has been enlisted in Table 1. The figure depicts the resonant peak loss (at certain spectral wavelength) of PCF based LSPR sensor that can be observed only when the phase matching condition is satisfied. The matching occurs only when the core guided mode energy (the leaky core mode) is transferred to the plasmonic mode and the resonant wavelength provides the peak loss in the respective cases. By varying sizes, shapes and refractive indices of the adjacent analyte media, the resonant conditions of LSPR

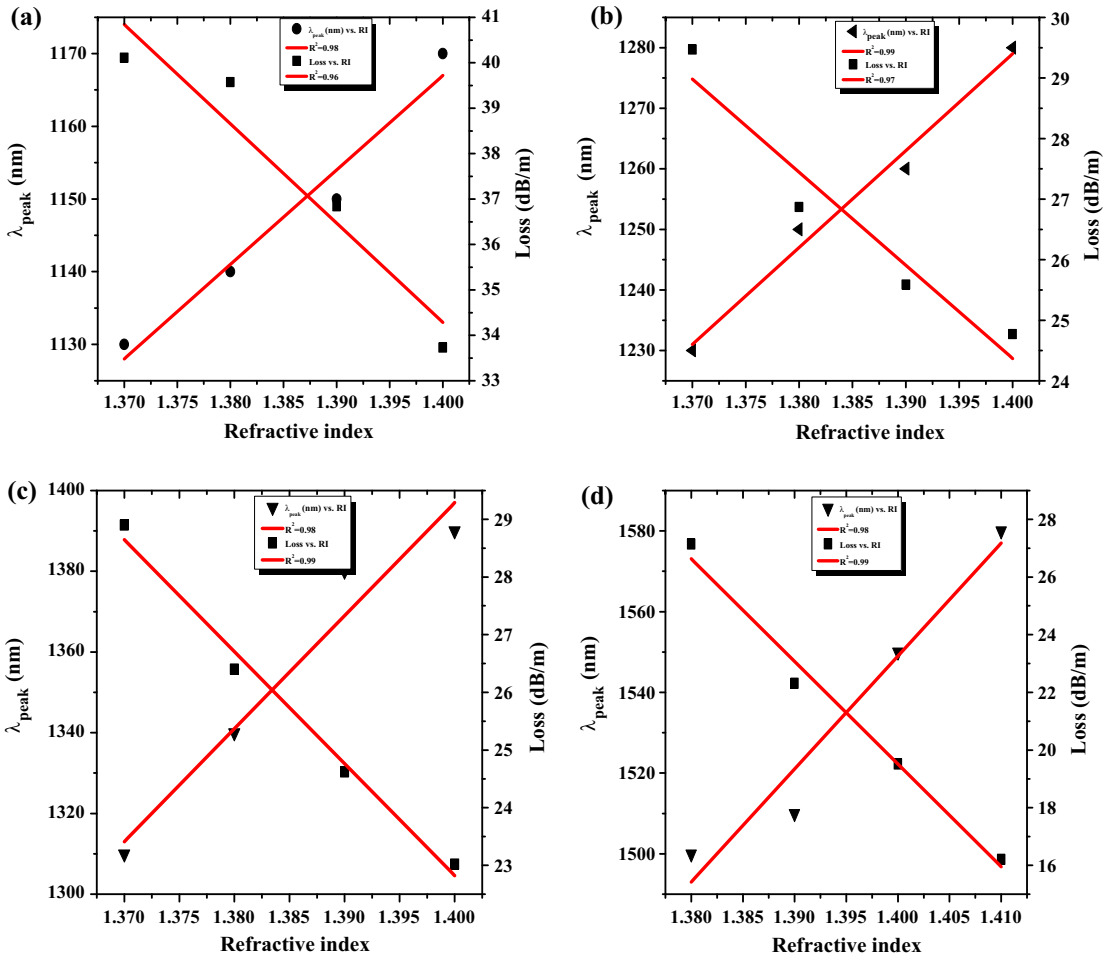

Fig. 5. Linear fitting curves for λ_{peak} and their corresponding loss vs. RI (1.37–1.40) of (a) 40 nm, (b) 50 nm, (c) 60 nm and (d) 70 nm nanospheres for crown based PCF.

based PCF sensor can be altered. The localized surface plasmons (LSPs) of the noble metal nanoparticle layer can be excited by the leaky core mode.

In Fig. 7 inset (a) represents the core guided mode in which the light is well confined to the core and inset (b) represents plasmon mode outside the resonant wavelength in which the light exists at the metal surface and also inset (c) represents the phase matching condition i.e., the coupling of fundamental core mode with that of plasmon mode with introduction of analyte of RI-1.32 in which the insets (a) denotes core mode (dashed line-green line), (b) implies plasmon mode (dotted line-red line) and (c) at resonance (solid line-blue line).

The sensing performance of LSPR-PCF has been calculated from Eqs. (2)–(4) which has been followed from Refs. [13,17–22]. The $\Delta\lambda_{peak}$ is the maximum peak shift in resonance wavelength for the respective RI indices and Δn_a is the variation in the RI of the proposed analytes, respectively. $\Delta\lambda_{min}$ is the minimum value that can be measured for a proposed LSPR-PCF. For the proposed structure, maximum peak shift is ~180 nm and Δn_a is considered to be as 0.01 and $\Delta\lambda_{min}$ is 0.1. Thus, the values of sensitivity, LOD and resolution are of the order of ~18,000 nm/RIU, $\sim 3.09 \times 10^{-10}$ and 5.56×10^{-6}, respectively. As shown in Eqs. (3) and (4) resolution and LOD depend upon $\Delta\lambda_{peak}$ which is the maximum possible peak wavelength and the results have been calculated for single analyte variation.

The results found in this study for this LSPR-PCF sensor based on different material domain reveal high precision and sensitivity to alteration of RI and sizes of the nanosphere. Although, we have presented the numerical analysis, the sensing scheme with inclusion of nanospheres in varying dimensions offer significant potential for implementation in biological and chemical applications. Minimal amount of modifications in the geometry of PCF, it can be introduced to analyze the sensing performance based on LSPR technique by varying sizes of nanospheres with inclusion of different analytes. Using this concept, one can fabricate a new class of PCF that can be applicable in variable sensing schemes.

4. Conclusion

In summary, we have demonstrated the working of a prototype LSPR-PCF sensor utilizing Au nanospheres embedded into a single layer of air holes. By changing sizes of nanosphere, the resonance has been observed by filling analytes with gradual rise in RI. During the analysis the step size for Δn_a (the variation in the RI of the proposed analytes) is considered to be as 0.01 and $\Delta\lambda_{min}$ (minimum value that can be measured by the proposed LSPR-PCF) is 0.1. The analysis has been performed in both material regime (*viz.* phosphate and crown PCF). During the study, highest sensitivity of ~18,000 nm/RIU has been observed for phosphate PCF with resolution of 5.56×10^{-6} (RIU) and LOD of 3.09×10^{-10}(RIU^2/nm) for 40 nm of Au nanosphere. Similarly, highest sensitivity for crown based PCF has been observed for 70 nm nanosphere ~27,000 nm/RIU with resolution and LOD nearly 3.7×10^{-6} (RIU) and 1.37×10^{-10} (RIU^2/nm). Additionally, it has been seen that sizes of the nanosphere have also influenced the spectral sensitivity of the sen-

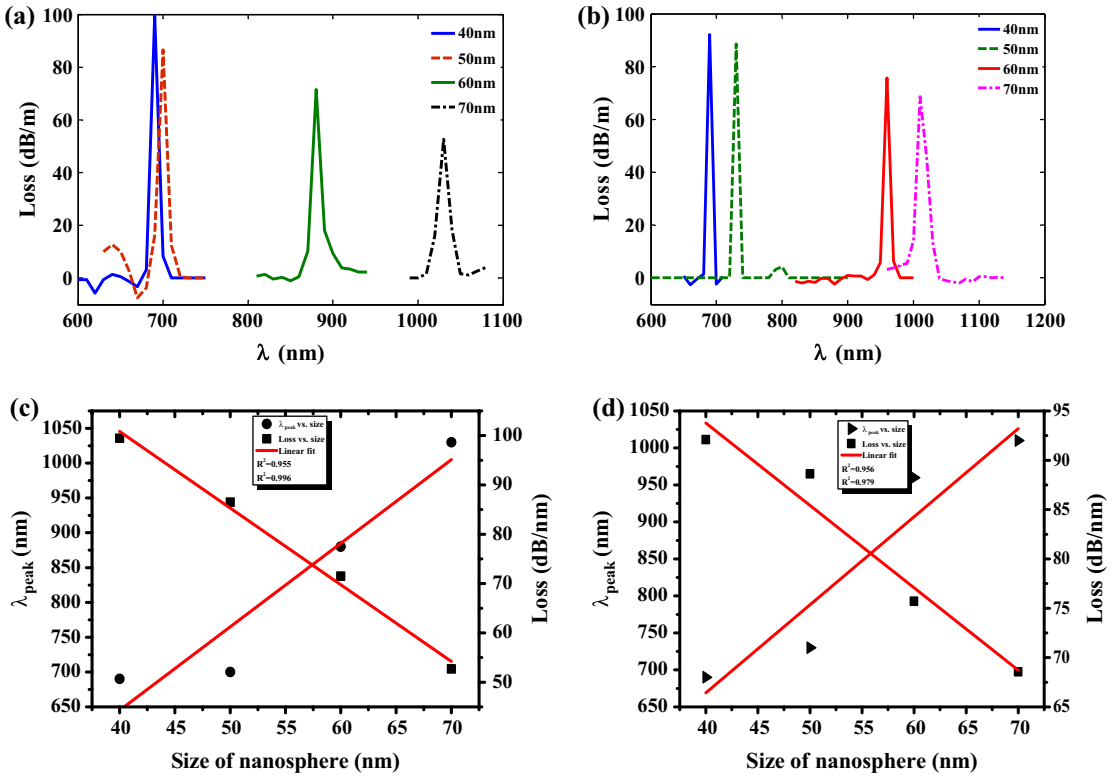

Fig. 6. Modal loss vs. λ (nm) of different sized nanosphere 40–70 nm for (a) Phosphate and (b) Crown based PCF, (c) peak value of loss and resonance wavelength vs. size of the nanosphere for Phosphate and (d) Crown based PCF.

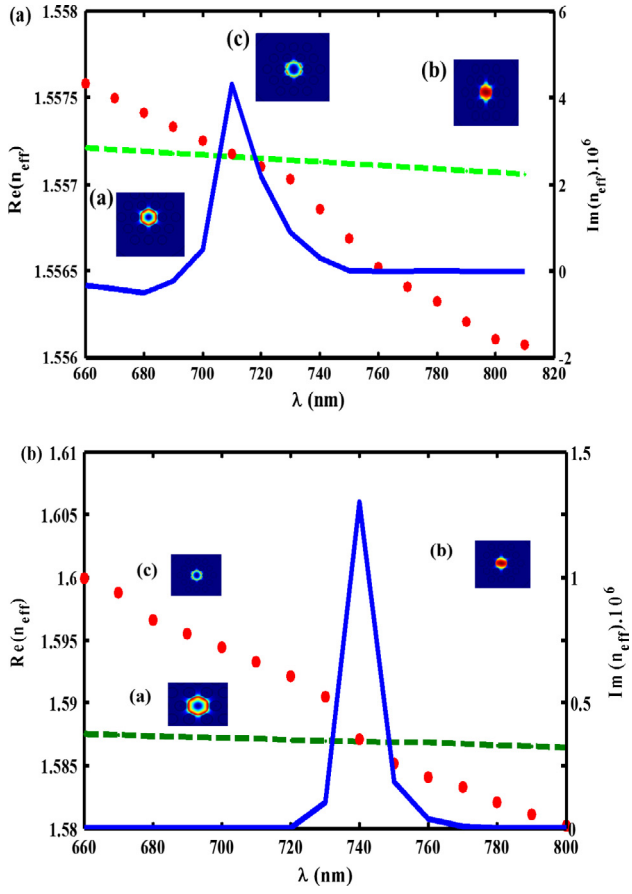

Fig. 7. Dispersion relation of core guided mode and surface plasmon mode (a) 40 nm phosphate PCF, (b) 40 nm Crown PCF (whereas insets (a) core mode, (b) at resonance and (c) plasmon mode).

sor. The modal loss in each case is found to diminish with increase in size of the Au nanosphere and peak wavelength is found to be red shifted with corresponding increment of refractive index of the analyte.

Acknowledgement

Author acknowledged Department of Physics and Department of Electronics and Communication Engineering for providing the facility to perform the simulation.

Appendix A. Supplementary material

Supplementary data associated with this article can be found, in the online version, at https://doi.org/10.1016/j.optlastec.2017.11.040.

References

[1] R. Bhardwaj, S. Mukherji, Gold nanoparticle coated U-bent fiber optic probe for localized surface plasmon resonance based detection of explosive vapors, Sens. Actuators B: Chem. 192 (2014) 804–811.
[2] J. Cao, E.K. Galbraith, T. Sun, K.T.V. Grattan, Comparison of surface plasmon resonance and localized surface plasmon resonance based optical fiber sensors, J. Phys. 307 (1) (2011) 1–7.
[3] H.Y. Lin, C.H. Huang, G.L. Cheng, et al., Tapered optical fiber sensor based on localized surface plasmon resonance, Opt. Express 20 (19) (2012) 21693–21701.
[4] C. Zhou, Localized surface plasmon resonance study of silver nano-cubes for photonic crystal fiber senor, Opt. Lasers Eng. 50 (2012) 1592–1595.
[5] X.C. Yang, Y. Lu, M.T. Wang, J.Q. Yao, A photonic crystal fiber glucose sensor filled with silver nanowires, Opt. Commun. 359 (2016) 279–284.
[6] P. Russell, Photonic crystal fiber, Rev. Appl. Phys. 299 (5605) (2003) 358–362.
[7] V.H. Aristizabal, F.J. Velez, P. Torres, Analysis of photonic crystal fibers: scalar solution and polarization correction, Opt. Express 14 (24) (2006) 11848–11854.
[8] K. Saitoh, M. Koshiba, Numerical modelling of photonic crystal fiber, IEEE JLT 23 (11) (2005) 3580–3590.

[9] D. Paul, R. Biswas, N.S. Bhattacharyya, Investigating photonic crystal fiber within E to L communication band with different material composites, Optik 126 (23) (2015) 4640–4645.
[10] D. Paul, R. Biswas, N.S. Bhattacharyya, Modal parameter analysis for crown glass and phosphate glass photonic crystal fiber, Indian J. Phys. 89 (7) (2015) 737–741.
[11] D. Paul, R. Biswas, N.S. Bhattacharyya, Predicting different losses of photonic crystal fibers in material and hetero-core domain, Opt. Mater. 48 (2015) 110–120.
[12] A.A. Rifat, G.A. Mahdiraji, Y.G. Shee, A novel photonic crystal fiber biosensor using surface plasmon resonance, Proc. Eng. 140 (2016) 1–7.
[13] A.A. Rifat, G.A. Mahdiraji, Y.M. Sua, et al., Highly sensitive multicore flat fiber surface plasmon resonance refractive index sensor, Opt. Express 24 (3) (2015) 2485–2495.
[14] Michele Midrio, Mukesh P. Singh, Carlo G. Someda, The space filling mode of holey fibers: an analytical vectorial solution, J. Lightwave Technol. 18 (7) (2000) 1031–1037.
[15] Y. Li, C. Wang, Y. Chen, M. Hu, B. Liu, L. Chai, Solution of the fundamental space-filling mode of photonic crystal fibers: numerical method versus analytical approaches, Appl. Phys. B 85 (2006) 597–601.
[16] L. Chao, W. Famei, L. Jingwei, et al., Design and theoretical analysis of a photonic crystal fiber based on surface plasmon resonance sensing, J. Nanophotonics 9 (1) (2015) 1–10.
[17] I.M. White, X. Fan, On the performance quantification of resonant refractive index sensors, Opt. Express 16 (2) (2008) 1020–1028.
[18] A.A. Rifat, G.A. Mahdiraji, D.M. Chow, et al., Photonic crystal fiber-based surface plasmon resonance sensor with selective analyte channels and graphene-silver deposited core, Sensors 15 (5) (2015) 11499–11510.
[19] X. Wang, S. Li, Q. Liu, et al., Design of a single-polarization single-mode photonic crystal fiber filter based on surface plasmon resonance, Plasmonics (2016), https://doi.org/10.1007/s11468-016-0390-3.
[20] Xia Yu, Ying Zhang, Shanshan Pan, Ping Shum, Min Yan, Yehuda Leviatan 4, Changming Li, A selectively coated photonic crystal fiber based surface plasmon resonance sensor, J. Opt. 12 (2010) 4p (015005).
[21] D. Paul, S. Dutta, R. Biswas, LSPR enhanced gasoline sensing with a U-bent optical fiber, J. Phys. D: Appl. Phys. 49(30) (2016) 1–10 (305104).
[22] D. Paul, S. Dutta, R. Biswas, LSPR based Ultra-sensitive low cost U-bent optical fiber for volatile liquid sensing, Sens. Actuators B: Chem. 250 (2017) 198–207.